Hindawi
Advances in Condensed Matter Physics
Volume 2023, Article ID 1754324, 13 pages
https://doi.org/10.1155/2023/1754324

Research Article

Unveiling the Robust Struct-Electromagnetic Characteristics of $CdAB_2$ Chalcopyrite (A = Cr, Mn, Fe; B = P, As): A Comprehensive *Ab-Initio* Study

D. Vijayalakshmi,[1,2] **Tholkappiyan Ramachandran**,[3] **G. Jaiganesh**,[4] **G. Kalpana**,[1] **and Fathalla Hamed**[3]

[1]*Department of Physics, College of Engineering, Anna University, Chennai 600 025, India*
[2]*Department of Physics, Vels Institute of Science, Technology & Advanced Studies (VISTAS), Pallavaram, Chennai, Tamil Nadu 600117, India*
[3]*Department of Physics, College of Science, United Arab Emirates University, Al-Ain P.O.X. 15551, UAE*
[4]*Excel Instruments, Gala No 9/10, Building No 2, Dias Industrial Estate, Vasai East Sativali Naka – 401208, India*

Correspondence should be addressed to D. Vijayalakshmi; vijayalakshmi.sbs@velsuniv.ac.in

Received 7 September 2023; Revised 11 October 2023; Accepted 24 October 2023; Published 21 November 2023

Academic Editor: Upendra Kumar

We present a comprehensive investigation of the electromagnetic properties of $CdAB_2$ compounds, where A represents Cr, Mn, or Fe, and B denotes P or As. To investigate the spin-polarized behavior of these compounds the A atoms were substituted at the Group IV (Ge) position in $CdGeB_2$ in the chalcopyrite crystal structure. Our results reveal that all the $CdAB_2$ compounds exhibit compelling spin-splitting of energy states near the Fermi level (E_F). Notably, $CdAB_2$ materials with A = Cr and Mn exhibit intriguing half-metallic ferromagnetic (HMF) characteristics, with the calculated total magnetic moments of 2.00 and 3.00 μ_B/f.u., respectively. The HMF properties originated in $CdAB_2$ (A = Cr and Mn; B = P, As) these compounds owing to the hybridization of partially filled -3d(t_{2g}) states of A atoms with the p-states of B (P, As) atoms, with minor contributions from Cd's-like states. In contrast, $CdFeB_2$ displays distinct behavior, demonstrating spin-splitting of energy levels around the E_F indicative of a stable ferromagnetic (FM) state and the absence of HMF at their equilibrium volume. The calculated total magnetic moments for $CdFeP_2$ and $CdFeAs_2$ are about 1.83 (1.64 μ_B/f.u.) and 1.94 μ_B/f.u. (1.84 μ_B/f.u.) under generalized gradient approximation (GGA) (local spin density approximation (LSDA)) approximations, respectively. Perhaps these $CdAB_2$ compounds (A = Cr and Mn; B = P, As) with HMF characteristic within both LSDA and GGA formalisms makes them highly promising candidates for spin injectors in the spintronic device applications. Furthermore, their semiconducting nature renders $CdCrB_2$ and $CdMnB_2$ materials compatible with silicon and other semiconducting lattices, enhancing their potential practical applications in the spintronic technologies. In conclusion, this study presents a thorough exploration of the robust electronic and magnetic properties of $CdAB_2$ chalcopyrites, offering exciting prospects for their utilization in the future spintronic applications.

1. Introduction

The quest for half-metallic ferromagnetic (HMF) materials with Curie temperature (T_C) surpassing room temperature has garnered significant attention for the potential spin-electronic device applications [1]. Many materials have been explored for their HMF properties, such as Ti-doped ZnS [2], Mn-doped InAs and GaAs [3], V-doped BeB (B = S, Se, Te) [4], CrB (B = S, Se, Te) [5, 6], $Mg_{1-x}V_xY$ (Y = Se, Te) [7], and Sc, Ti, V, Mn, and Cr-doped CdS [8]. These systems exhibit HMF behavior due to the substitution of transition metal (TM) ions, inducing small local magnetic moments in the nonmagnetic host materials with T_C up to 200 K [3, 9]. Consequently, they have attracted great interest in spintronic applications [1–8]. However, their T_C does not exceed 200 K [3], making them less favorable for applications in spin-based solid-state devices.

For practical spintronic applications, materials displaying room-temperature ferromagnetism (FM) are highly preferred.

Ternary II–IV–V_2 semiconductors, crystallizing in the body-centered tetragonal (BCT) chalcopyrite structure with the space Group I-42d, have emerged as promising candidates for various technological applications [10–13]. By replacing a small fraction of constituent atoms with TM ions such as Cr or Mn, II–IV–V_2 materials can be engineered for spintronic purposes. The doping of TM ions induces a strong spin splitting of energy levels around the Fermi level (E_F) with relatively high T_C [10–14]. The appearance of HMF property relies on the concentration of magnetic ions and temperature. Experimental results have revealed room temperature FM ($T_C = 320$ K) in Mn-doped $CdGeP_2$ due to the high-carrier solubility of Mn atoms in $CdGeP_2$, where Mn^{2+} easily occupies the divalent Cd site without altering electrical neutrality.

The substitutional site of TM ions in ternary compounds plays a crucial role in determining FM or antiferromagnetic (AFM) properties. When M (A = Mn, Cr, or V) atoms are substituted at the Group II (divalent) site of Ternary II–IV–V_2 chalcopyrite, AFM spin arrangement is favored. Conversely, when the same M atoms are substituted at the tetravalent (Group IV) site, FM configuration with hole formation is observed [15]. Notably, stable FM states have been achieved with $T_C = 355$ K by substituting Mn at the Ge site in $CdGeP_2$, making the experimental fabrication of such materials feasible. Moreover, TM-doped or replaced chalcopyrite (II–IV–V_2) semiconductors have been shown to exhibit FM above room temperature, drawing attention in the field of spintronics [13, 14, 16, 17].

Theoretical and experimental results have demonstrated room-temperature FM ($T_C = 320$ and 340 K, respectively) in $MnGeP_2$ and $MnGeAs_2$ chalcopyrite materials [13, 17–19], motivating us to conduct first-principles calculations on the structural, electronic, and magnetic properties of $CdAB_2$ (A = Cr, Mn, Fe; B = P, As) chalcopyrite's.

Building on the previous research, [19, 20] which explored spin-polarized calculations on $ZnMX_2$ (A = Sc, Ti, V, Cr, Mn, Fe; X = P, As) and $CdAB_2$ (A = Sc, Ti, V; X = P, As) compounds, revealing the possibility of FM upon M atom substitution at the Ge site of II(Zn/Cd)IV(Ge)–VI(P/As)$_2$ compounds, our present work extends this study by substituting M atoms (A = Cr, Mn, Fe) at the Ge site of $CdGeX_2$. Utilizing the full-potential linearized augmented plane wave (FP-LAPW) method with two correlation functionals, generalized gradient approximation (GGA) [21] and local spin density approximation (LSDA) [22, 23], we investigate the introduction of deep levels by TM impurities in the band gap of $CdGeB_2$ semiconductors, resulting in attractive electronic and magnetic properties in these chalcopyrite's. To understand the magnetic states of $CdAB_2$ compounds, we perform total energy vs. volume calculations for NM, FM, and AFM phases. Additionally, we present spin-dependent band structures, charge density plots, and density of states (DOS) at equilibrium conditions for all the compounds.

This study contributes to the growing understanding of robust room temperature ferromagnetism in $CdAB_2$ chalcopyrite through transition metal substitution, offering valuable insights for the potential spintronic applications.

2. Method of Calculation and Crystal Structure

In this study, we conducted first-principal calculations using the Full-Potential Linearized Augmented Plane Wave (FP-LAPW) method [22], known for its accuracy in electronic structure calculations of the periodic solids. The WIEN2k code [24] was employed for the calculations of the structural, electronic, and magnetic properties of $CdAB_2$ compounds. Both GGA [24] and LSDA [22] were used for the exchange-correlation functions in these calculations.

The FP-LAPW technique employs a muffin-tin potential to represent the crystal potential. This assumes that the crystal potential is spherically symmetric within the muffin-tin sphere and remains constant in the interstitial space. The core electrons within the atomic sphere are treated with full relativistic considerations and self-consistency using a spherical approximation. Meanwhile, the valence electrons in the interstitial region are treated as self-consistently as possible, but with a semi-relativistic approach. Inside the atomic sphere, the crystal potential, electronic wave functions, and charge density are expanded using spherical harmonics up to a maximum angular momentum quantum number of $l_{max} = 10$. In the interstitial region, a Fourier series of plane waves is employed, with a cutoff defined as the product of the muffin-tin radius (RMT) and the maximum wave vector (K_{max}), set to 7.0. For specific elements like Cd, Cr, Mn, Fe, P, and As, atomic sphere radii are designated as 2.08, 2.23, 2.24, 2.17, 2.20, and 2.09, respectively. The charge density is expanded in a Fourier series up to a maximum reciprocal lattice vector denoted as Gmax = 12. To integrate over k-points in the irreducible wedge of the first Brillouin zone, an $8 \times 8 \times 4$ k-mesh is used. Through an iterative process, the crystal's self-consistent total energy is brought to convergence, achieving a value lower than 0.01 m Ry.

$CdGeB_2$ semiconductor adopts the chalcopyrite structure with BCT lattice type and space group I-42d (122). The atomic positions of the atoms are as follows: Cd_1 (0, 0, 0), Cd_2 (0, 1/2, 1/2); Ge_1 (1/2, 1/2, 0); Ge_2 (1/2, 0, 1/4), B_1 (u, 1/4, 1/8); B_2(u, 3/4, 1/8); B_3 (3/4, u, 7/8); B_4 (1/4, u, 7/8), where u represents the anion displacement (internal parameter). Ternary $CdAB_2$ (A = Cr, Mn, Fe; B = P, As) compounds are derived from $CdGeB_2$ by replacing Ge with 3d TM (Cr, Mn, Fe) ions. The ionic, atomic radii and electronegativities of M [25] atoms are compared to Ge, ensuring the retention of the chalcopyrite crystal structure for the all substituents (A = Cr, Mn, Fe) in $CdGeB_2$ compounds. In the chalcopyrite structure, each B (P/As) anion is coordinated with two Cd and two Ge/M cations, while each cation is tetrahedrally coordinated by four B (P/As) anions. Slight displacement of the anions from their ideal tetrahedral site results in two unequal cation–anion bond lengths. Maintaining the tetragonal distortion $\eta = c/2a \sim 1$ as in CdG_2, the chalcopyrite crystal symmetry is preserved in all $CdAB_2$ compounds.

3. Results and Discussion

Before delving into electronic and magnetic properties, we performed full structural optimization for the $CdAB_2$

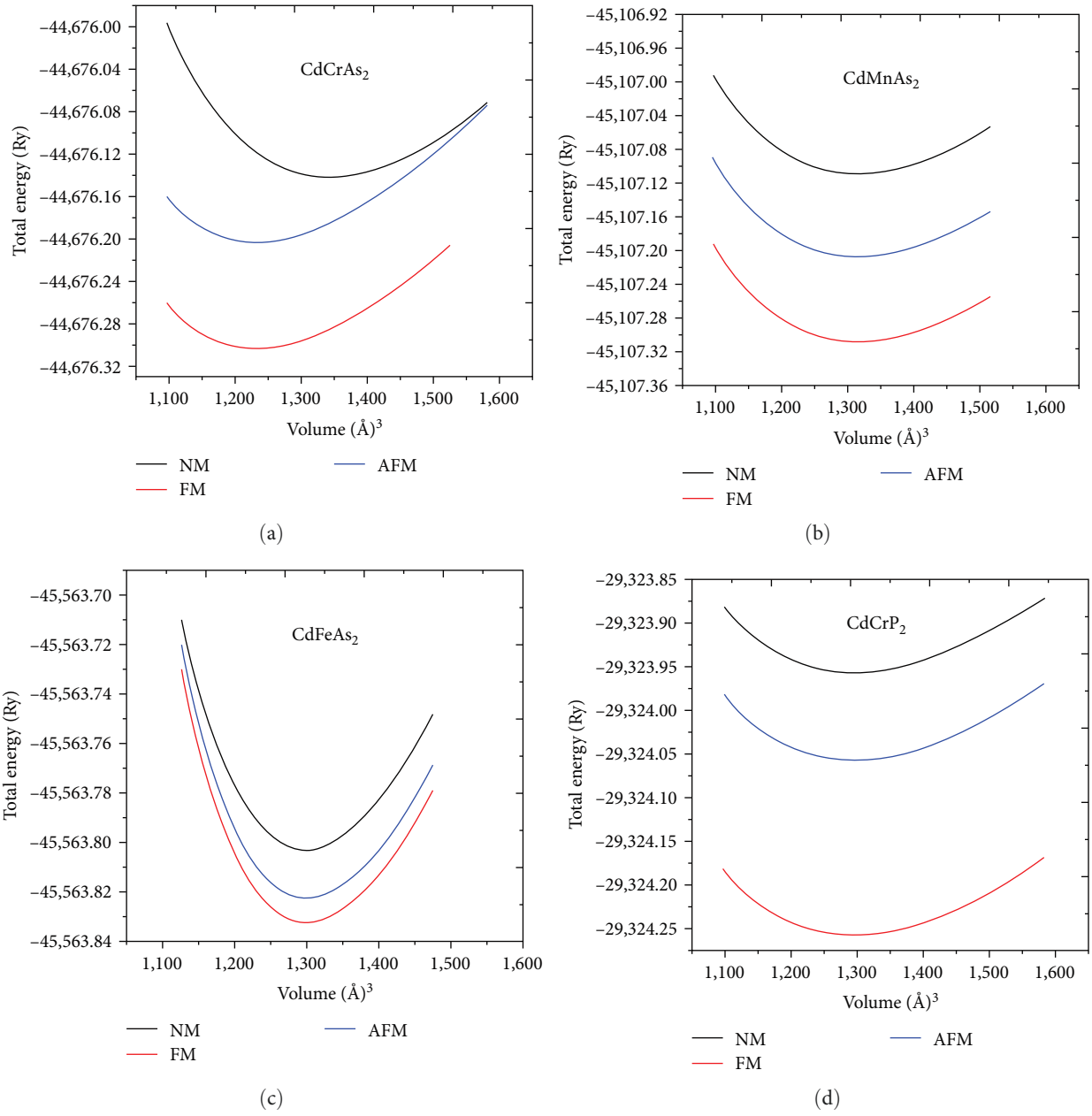

Figure 1: Continued.

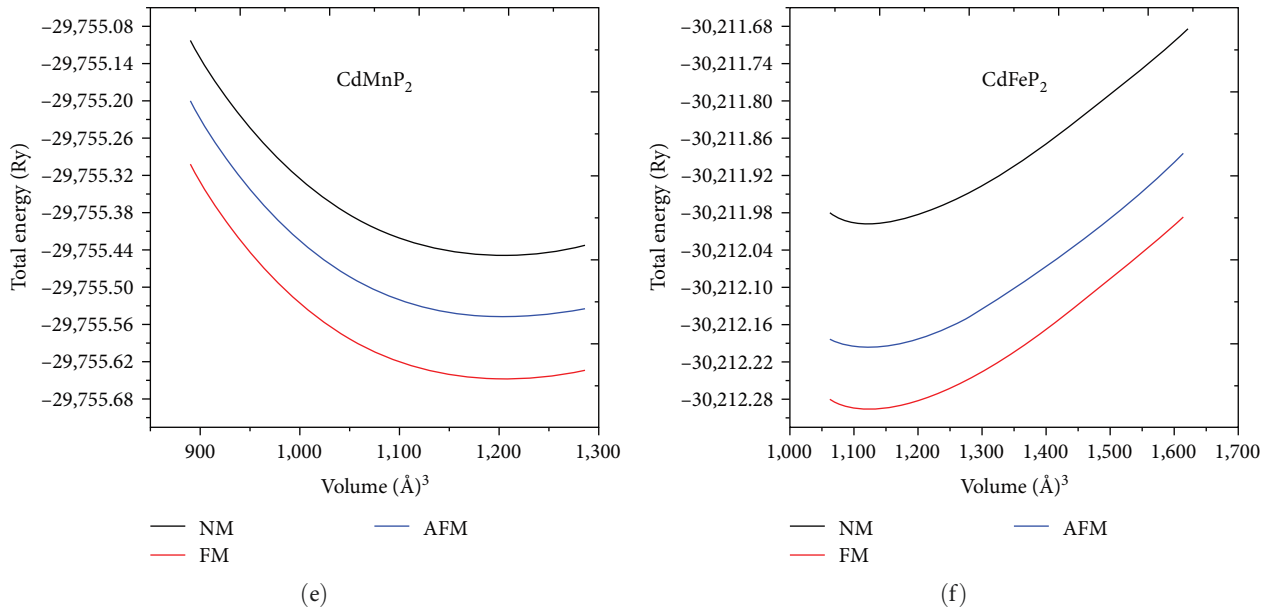

FIGURE 1: Total energy (in Ry) per formula unit as a function of volume (in Å^3) plots for the nonmagnetic (NM), ferromagnetic (FM), and antiferromagnetic (AFM) phases of $CdMP_2$ (M = Cr, Fe) compounds using the generalized gradient approximation (GGA).

(A = Cr, Mn, Fe; B = P, As) compounds. The chalcopyrite structure (BCT phase) with space group I-42d (# No. 122) was described using unit cell lattice parameters (a_o, c_o) and one internal parameter (u). Structural optimization was carried out for all compounds within both the GGA and LSDA for the nonmagnetic (NM), ferromagnetic (FM), and antiferromagnetic (AFM) phases. Since the results obtained under GGA and LSDA schemes were found to be identical, the calculated total energy as a function of the lattice parameter for GGA is represented in Figure 1.

To determine the equilibrium values of u, a_o, c_o, and bulk modulus (B_o) of $CdAB_2$, the total energies were fitted to Birch–Murnaghan's equation of state [26] as a function of relative volume within GGA and LSDA for the NM, FM, and AFM states of each compound. The calculated values of u, a_o, c_o, and B_o for $CdGeB_2$ and $CdAB_2$ compounds are presented in Tables 1 and 2. Remarkably, the calculated ground state properties of $CdGeB_2$ are in excellent agreement with the experimental and previously reported results [27]. However, it is noted that the calculated lattice constants are overestimated by GGA and underestimated by LSDA, as expected. The internal parameter u was found to vary from 0.268 to 0.306, as observed from the tables.

Figure 1 showcases the total energy–volume curves of $CdAP_2$ and $CdAAs_2$ (A = Cr, Mn, Fe) compounds under GGA approximation. The energy–volume curves for $CdAB_2$ (A = Cr, Mn, Fe; B = P, As) compounds indicate that the FM phase exhibits the minimum energy, signifying their ferromagnetic stability at equilibrium. To further assess the stability of the magnetic state, we calculated the spin-polarized energy differences ΔE_1 ($\Delta E_1 = E_{FM} - E_{NM}$) and ΔE_2 ($\Delta E_2 = E_{FM} - E_{AFM}$), i.e., the energy gains due to the formation of magnetic moments in the systems. The negative values of total energy differences ΔE_1 and ΔE_2 for $CdAB_2$ (M = Cr, Mn, Fe) compounds indicate the desirability of the FM state in these materials. The calculated total energy differences ΔE_1 and ΔE_2 under GGA and LSDA can be found in Tables 1 and 2.

The equilibrium bulk modulus (B_o) values of $CdAB_2$ (A = Cr, Mn, Fe; B = P, As) compounds were calculated for their NM, FM, and AFM phases using Equation (1) [28]. The calculated B_o values are presented in Tables 1 and 2 under the GGA and LSDA schemes.

$$B_0 = -V_0[dp/dv]\,. \tag{1}$$

Bulk modulus is a crucial mechanical property that characterizes a material's resistance to volume changes during expansion or compression. With the substitution of transition metal (TM) atoms in the host $CdGeB_2$ compounds, the lattice parameters (a_o, c_o) may increase or decrease, leading to corresponding changes in the B_o values due to the displacement of the electric charge of core electrons via valence electrons. Notably, GGA tends to yield larger lattice parameters and smaller bulk modulus values compared to the LSDA.

The chalcopyrite crystal structure is a superlattice of the zinc blende (ZnS) structure. Doubling the unit cell of ZnS results in a change in the anion As/P position along the z-direction. This leads to tetragonal distortion in $CdAB_2$ compounds, forming different bond lengths. The relaxed anion–cation bond lengths ($R_{Cd\text{-}X}$ and $R_{M\text{-}X}$) for the host $CdGeB_2$ and $CdAB_2$ compounds were calculated for the NM, FM, and AFM states using Equations (2) and (3) [29] under GGA and LSDA and are presented in Tables 3 and 4.

$$R_{Cd-X} = a\left[u^2 + \frac{(1+\eta^2)}{16}\right]^{1/2}, \tag{2}$$

Table 1: Calculated internal parameter (u), equilibrium lattice constants (a_0, c_0) in Å, and bulk modulus (B_0) in GPa, total energy difference ΔE_1 ($\Delta E_1 = E_{FM} - E_{NM}$) in meV/cell, ΔE_2 ($\Delta E_2 = E_{FM} - E_{AFM}$) in meV/cell between the nonmagnetic (NM), ferromagnetic (FM), and antiferromagnetic (AFM) states of $CdAB_2$ (M = Cr, Mn, Fe; B = P, As) using generalized gradient approximation (GGA).

Compounds	NM				FM				AFM				ΔE_1 (meV)	ΔE_2 (meV)
	u	a_0 (Å)	c_0 (Å)	B_0 (GPa)	u	a_0 (Å)	c_0 (Å)	B_0 (GPa)	u	a_0 (Å)	c_0 (Å)	B_0 (GPa)		
$CdGeP_2$	0.279	6.326	11.88	79.04	0.279	6.326	11.88	79.04	0.279	6.326	11.88	79.04	–	–
Others	0.283[a]	5.740[a]	10.77[a]											
$CdCrP_2$	0.303	5.84	11.05	76.03	0.302	5.86	11.07	55.34	0.301	5.89	11.05	61.09	−1.3	−6.8
$CdMnP_2$	0.308	5.67	10.73	78.12	0.285	5.69	10.76	70.52	0.302	5.71	10.78	75.65	−9.6	−5.3
$CdFeP_2$	0.301	5.62	10.56	95.01	0.300	5.60	10.58	95.08	0.308	5.62	10.60	93.28	−8.6	−5.5
$CdGeAs_2$	0.280	6.12	11.31	65.37	0.280	6.12	11.31	59.56	0.280	6.12	11.31	59.04	–	–
Others	0.278[a]	5.94[a]	11.216[a]											
$CdCrAs_2$	0.307	6.04	11.35	64.46	0.306	6.02	11.37	55.73	0.305	6.04	11.35	59.04	−2.66	−2.49
$CdMnAs_2$	0.304	5.93	11.18	69.50	0.303	5.91	11.16	66.66	0.301	5.93	11.18	63.78	−9.51	−1.87
$CdFeAs_2$	0.302	5.89	11.11	79.75	0.301	5.87	11.09	65.89	0.308	5.89	11.08	78.77	−5.63	−5.94

[a]Thorpe & Pamplin (1968).

Table 2: Calculated internal parameter (u), equilibrium lattice constants (a_0, c_0) in Å, and bulk modulus (B_0) in GPa, total energy difference ΔE_1 ($\Delta E_1 = E_{FM} - E_{NM}$) in meV/cell, ΔE_2 ($\Delta E_2 = E_{FM} - E_{AFM}$) in meV/cell between the nonmagnetic (NM), ferromagnetic (FM), and antiferromagnetic (AFM) states of $CdAB_2$ (M = Cr, Mn, Fe; B = P, As) using local spin density approximation (LSDA).

Compounds	NM				FM				AFM				ΔE_1 (meV)	ΔE_2 (meV)
	u	a_0 (Å)	c_0 (Å)	B_0 (GPa)	u	a_0 (Å)	c_0 (Å)	B_0 (GPa)	u	a_0 (Å)	c_0 (Å)	B_0 (GPa)		
$CdGeP_2$	0.268	5.89	11.04	69.04	0.302	**5.82**	11.18	71.04	0.279	5.85	11.08	79.01	-	-
$CdCrP_2$	0.304	5.43	10.78	112.6	0.302	5.76	10.88	78.35	0.303	5.41	10.76	98.34	−9.4	−9.4
$CdMnP_2$	0.301	6.18	11.41	123.45	0.301	5.70	10.78	83.81	0.302	6.19	11.56	81.04	−4.1	−4.3
$CdFeP_2$	0.306	5.42	11.29	144.78	0.303	5.56	10.50	114.8	0.307	5.48	11.31	101.96	−5.81	−6.16
$CdGeAs_2$	0.301	5.98	10.98	61.77	0.302	5.92	11.21	56.56	0.304	5.91	11.01	58.04	–	–
$CdCrAs_2$	0.301	5.74	10.84	97.81	0.301	5.97	11.29	56.03	0.304	5.72	10.78	92.30	−7.2	−6.2
$CdMnAs_2$	0.303	5.56	11.04	91.09	0.303	5.79	10.94	83.85	0.304	5.35	10.96	89.78	−16.8	−4.8
$CdFeAs_2$	0.301	5.42	11.13	86.94	0.307	5.77	10.91	82.05	0.306	5.41	11.11	88.60	−7.3	−9.48

Table 3: Calculated heat of formation (ΔH) in eV and bond length in Å for $CdAB_2$ (M = Cr, Mn, Fe; B = P, As) compounds using generalized gradient approximation (GGA).

Compounds	NM			FM			AFM		
	ΔH (eV)	Bond length (Å)		ΔH (eV)	Bond length (Å)		ΔH (Å)	Bond length (Å)	
		Cd-Y	M-Y		Cd-Y	M-Y		Cd-Y	M-Y
$CdGeP_2$	−29.74	2.65	2.65	−29.56	2.68	2.68	−30.71	2.66	2.66
$CdCrP_2$	−30.3	2.34	2.24	−30.5	2.14	2.04	−29.6	2.12	2.02
$CdMnP_2$	−25.9	2.33	2.23	−25.7	2.13	2.03	−30.8	2.11	2.01
$CdFeP_2$	−37.9	2.48	2.48	−37.7	2.28	2.28	−25.4	2.24	2.24
$CdGeAs_2$	−43.87	2.53	2.53	−44.34	2.52	2.52	−48.76	2.52	2.52
$CdCrAs_2$	−45.1	2.28	218	−45.3	2.28	218	−49.6	2.24	2.12
$CdMnAs_2$	−17.6	2.46	2.36	−17.4	2.11	2.06	−45.5	2.18	2.04
$CdFeAs_2$	−51.8	2.37	2.47	−51.6	2.13	2.27	−17.6	2.11	2.25

Table 4: Calculated heat of formation (ΔH) in eV and bond length in Å for $CdAB_2$ (M = Cr, Mn, Fe; B = P, As) compounds using local Spin Density Approximation (LSDA).

Compounds LSDA	NM			FM			AFM		
	ΔH (eV)	Bond length (Å)		ΔH (eV)	Bond length (Å)		ΔH (eV)	Bond length (Å)	
		Cd-Y	M-Y		Cd-Y	M-Y		Cd-Y	M-Y
$CdGeP_2$	−34.13	2.63	2.63	−34.76	2.63	2.63	−34.98	2.61	2.61
$CdCrP_2$	−34.97	2.36	2.25	−34.67	2.38	2.23	−34.69	2.40	2.36
$CdMnP_2$	−42.46	2.22	2.11	−42.48	2.24	2.23	−42.51	2.26	2.15
$CdFeP_2$	−57.83	2.15	2.22	−57.85	2.15	2.09	−57.87	2.17	2.24
$CdGeAs_2$	−36.23	2.51	2.51	−35.47	2.48	2.48	−36.47	2.46	2.46
$CdCrAs_2$	−36.82	2.43	2.32	−36.84	2.45	2.30	−36.87	2.47	2.32
$CdMnAs_2$	−35.62	2.37	2.25	−35.64	2.39	2.23	−35.65	2.41	2.25
$CdFeAs_2$	−31.08	2.22	2.33	−31.09	2.24	2.35	−31.12	2.26	2.47

$$R_{M-X} = a\left[\left(u - \frac{1}{2}\right)^2 + \frac{(1+\eta^2)}{16}\right]^{1/2}. \quad (3)$$

$$\Delta H = \frac{1}{a+b+c}\left[E_{\text{Total}}^{\text{CdMX}} - aE_{\text{Solid}}^{\text{Cd}} - bE_{\text{Solid}}^{\text{M}} - 2cE_{\text{Solid}}^{\text{X}}\right]. \quad (4)$$

In $CdAB_2$ compounds with M = Cr and Mn, the calculated bond length $R_{M\text{-}B}$ is shorter than $R_{Cd\text{-}B}$ due to the larger electronegativity of B [22] atoms. Consequently, the M atoms move closer to the B atom, resulting in decreased $R_{M\text{-}B}$ in these compounds with u values > 0.25. Conversely, for $u < 0.25$, $R_{Cd\text{-}B}$ becomes reduced compared to $R_{Fe\text{-}B}$ in $CdFeB_2$, where $R_{Fe\text{-}B}$ increases due to the decrease in the electro-positivity of Fe atoms. In this case, the Cd atom moves toward the B atom. It is important to highlight that bond lengths exhibit a reduction in the GGA method as opposed to the LSDA approach. This reduction in bond lengths intensifies the rigidity among Cd, M, and B atoms and amplifies the electron concentration in the valence area. In order to enhance our comprehension of electron behavior within the valence region, additional calculations were performed to determine the compounds' band structure, density of states (DOS), and electron charge density.

Additionally, the heat of formation (ΔH) for all the $CdAB_2$ compounds in the NM, FM, and AFM phases were calculated using Equation (4) [29], and the results are provided in Tables 3 and 4.

The computed ΔH (enthalpy) values were discovered to be negative using both the LSDA and GGA methodologies. This signifies that all the compounds are expected to be thermodynamically stable in the chalcopyrite structure. These findings provide valuable insights into the mechanical and thermodynamic stability of $CdAB_2$ chalcopyrite, contributing to a deeper understanding of their potential applications in various fields of materials science.

The spin-resolved electronic band structures of $CdAB_2$ compounds (where A = Cr, Mn, Fe, and B = P, As) were computed along high-symmetry directions within the first Brillouin zone at their equilibrium volume using both the GGA and LSDA. Electronic band structures for $CdAB_2$ compounds (A = Cr, Fe; B = P, As) are depicted in Figures 2 and 3 for the GGA approach. These figures illustrate the overall profile of the band structure, which remains quite similar for all $CdAB_2$ compounds under both approximations. The introduction of -d states near the Fermi level (E_F) due to the substitution of elements A = Sc, Ti, V, Cr, Mn, and Fe in the $ZnGeB_2$ structure leads to a crystal field resonance. This resonance causes a splitting of the -d states into

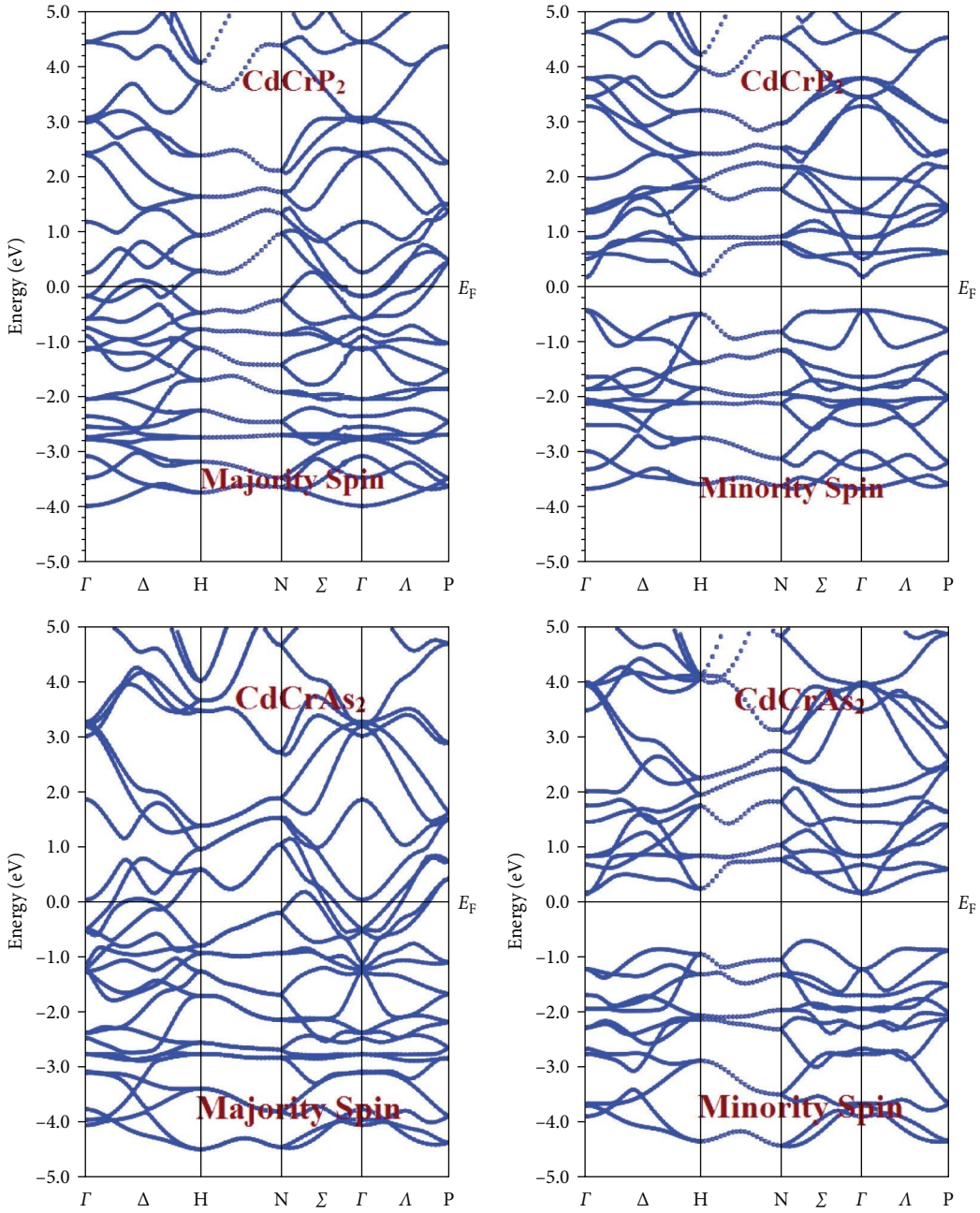

FIGURE 2: Spin-polarized electronic band structures of $CdCrP_2$ using the generalized gradient approximation (GGA).

suborbitals labeled as "eg" and "t_{2g}". As a result of the hybridization between -d states and -p states from the nearest neighboring B atom, an indirect band gap emerges in the spin-down channel. Meanwhile, the, eg and t_{2g} states within the majority spin channel intersect the Fermi level, indicating a HMF characteristic within these compounds.

Figure 2 illustrates the spin-polarized band structure of $CdCrP_2$, highlighting the noticeable spin polarization of energy states in the vicinity of the Fermi level (E_F). Specifically, the bonding -3d, eg states and the anti-bonding t_{2g} states associated with the Cr atom is notably concentrated near the EF. This arrangement results in the formation of an indirect band gap between the valence band maximum (VBM) and the conduction band minimum (CBM) within the spin-down channel. In contrast, in the spin-up channel, the e_g, t_{2g} states of the -3d Cr atom and -3p states of P atoms extend and cross the E_F, leading to HMF nature in this compound. Similar phenomena were observed in $CdCrAs_2$ and $CdMnB_2$ (B = P, As) compounds. The calculated HMF gap (E_{HM}) and spin-splitting energy gaps ($E_g\downarrow$) of $CdAB_2$ (A = Cr, Mn; B = P, As) are listed in Table 5 for both GGA and LSDA.

On the other hand, $CdFeP_2$ (Figure 3) shows spin-splitting of energy levels around the E_F, indicating the occurrence of stable ferromagnetism. However, the VBM crosses the E_F in both the spin-up and spin-down channels, signifying

Table 5: Calculated half-metallic gap (E_{HM}) in eV, minority spin gap ($E_g\downarrow$) in eV, partial, interstitial, and total magnetic moments in μ_B for $CdAB_2$ (M = Cr, Mn, Fe; B = P, As) compounds at their equilibrium volume using generalized gradient approximation (GGA) and local spin density approximation (LSDA).

Compounds	GGA							LSDA						
	E_{HM} (eV)	$E_{g\downarrow}$ (eV)	Magnetic moments (μ_B)					E_{HM} (eV)	$E_{g\downarrow}$ (eV)	Magnetic moments (μ_B)				
			Cd	M	Y	Int.	Total			Cd	M	Y	Int.	Total
$CdCrP_2$	0.948	0.54	0.042	1.979	−0.132	0.655	**2.00**	0.405	0.42	0.032	1.479	−0.132	0.655	**2.00**
$CdMnP_2$	0.880	0.40	0.043	2.54	−0.13	0.46	**3.00**	0.525	0.75	0.033	2.14	−0.13	0.46	**3.00**
$CdFeP_2$			0.018	1.862	−0.022	0.26	2.49			0.010	1.462	−0.022	0.26	2.28
$CdCrAs_2$	1.153	0.60	0.009	2.088	−0.056	0.153	**2.00**	0.424	0.93	0.006	1.888	−0.046	0.143	**2.00**
$CdMnAs_2$	0.884	0.16	0.040	3.545	−0.074	0.163	**3.00**	0.696	0.86	0.020	3.145	−0.064	0.123	**3.00**
$CdFeAs_2$			0.003	1.932	−0.031	0.079	2.83			0.001	1.932	−0.021	0.069	2.63

Note. The integer magnetic moment shows the characteristic of half-metallic ferromagnetism which is indicated in bold.

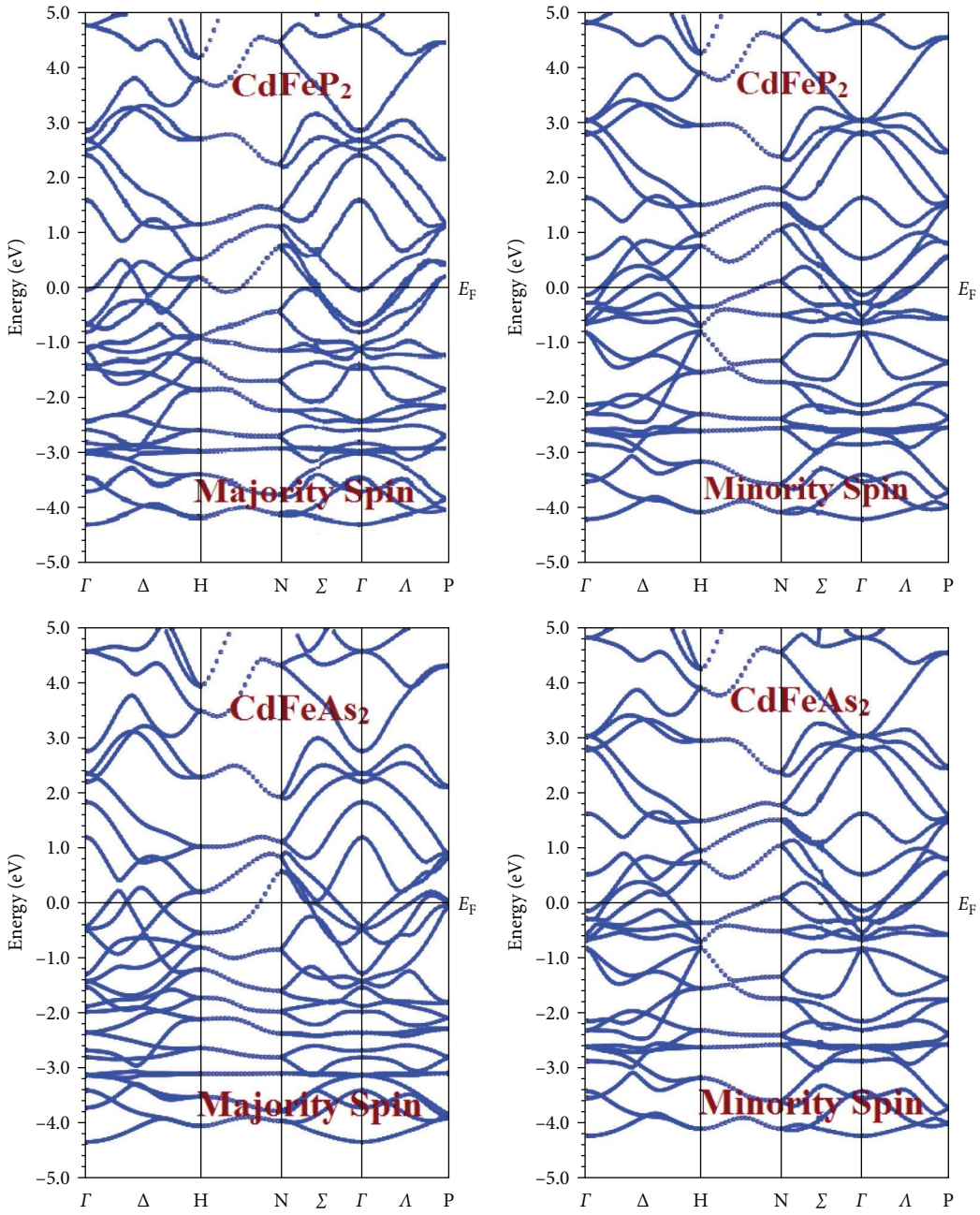

Figure 3: Spin-polarized electronic band structure of $CdFeP_2$ using the generalized gradient approximation (GGA).

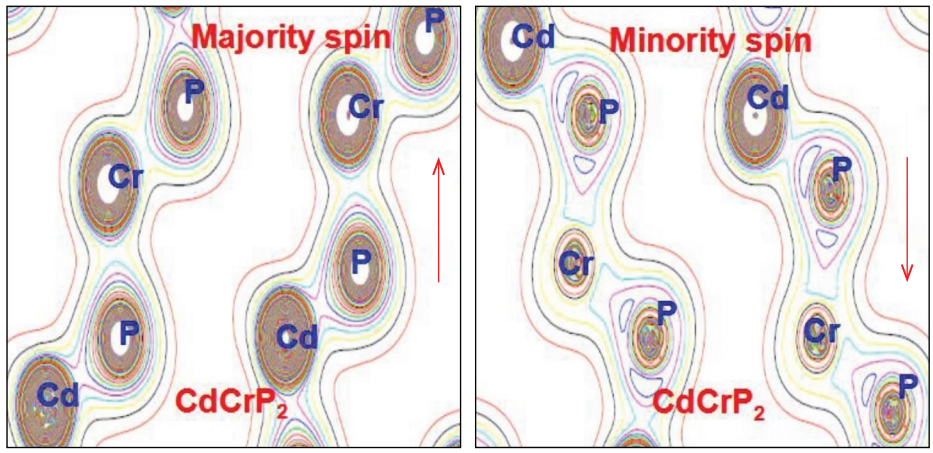

FIGURE 4: Valence electron charge density contour plots in the (110) plane for $CdCrP_2$ using the generalized gradient approximation (GGA).

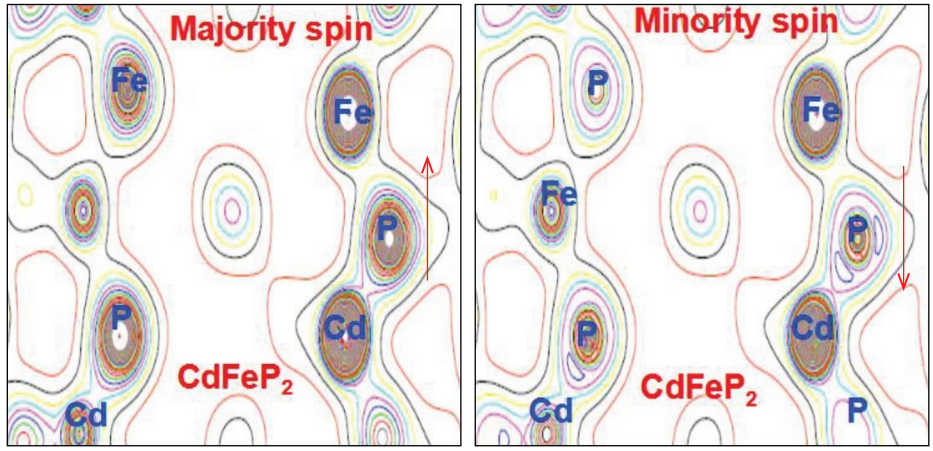

FIGURE 5: Valence electron charge density contour plots in the (110) plane for $CdFeP_2$ using the generalized gradient approximation (GGA).

the absence of HMF property in these compounds. The decrease in exchange spin-splitting energy is attributed to the coupling of magnetic t_{2g} and e_g suborbital of -3d states of Fe atoms and the repulsion between the -3d (t_{2g} and e_g) states of Fe and -p states of P atoms in the VBM. This leads to an increase in the VB width, reducing the localization of the electron in the VB region and increasing the spin-polarization around the E_F.

The charge density contour plots (Figures 4 and 5) offer insight into the chemical bond nature in $CdAP_2$ (A = Cr, Fe) compounds. The plots provide evidence of charge transfer involving valence electrons shifting from Cd to P and from M to P ions. This transfer signifies a blend of both ionic and covalent attributes in the atomic bonds between Cd-P and M-P, holding for both spin channels across all compounds. An examination of the electronic charge distribution surrounding the P atom reveals the establishment of Cd-P and M-P bonds. Particularly strong p-d exchange interactions between Cr (d) and P (p) states are evident, driving a substantial covalent character between P and Cr within $CdCrP_2$. Likewise, the compounds $CdCrAs_2$ and $CdMnB_2$ (where B = P, As) showcase pronounced charge transfer between M and P ions. This results in a robust p-d(t_2g) interaction between the band carriers and localized spins, leading to a HMF nature in these compounds.

Total and partial density of states (PDOS) calculations (Figures 6 and 7) for $CdCrP_2$ and $CdFeP_2$ within GGA reveal significant changes in the DOS near the E_F, leading to spin-polarization of the valence bands (VBs). In $CdCrP_2$, the e_g orbitals are well-localized and form an indirect band gap between the VB and CB in the spin-down channel. In the spin-up channel, the t_{2g} states cross the E_F, leading to HMF behavior. A similar phenomenon was observed in $CdCrAs_2$ and $CdMnB_2$ (B = P, As), where the p-d (t_{2g}) states of B and A (Cr, Mn) atoms play a dominant role in the formation of the gap between valence and conduction bands in the spin-down channel.

Conversely, $CdFeP_2$ and $CdFeAs_2$ do not exhibit HMF behavior, as the strong overlapping and repulsive reaction between -3d states of Fe (e_g and t_{2g}) and -p states of P/As reduce the magnetic moment of Fe, resulting in spin-splitting of energy states around the E_F without an observed band gap in the minority spin channel.

Using the spin-polarized calculations, the total and local magnetic moments of $CdAB_2$ compounds (where A = Cr,

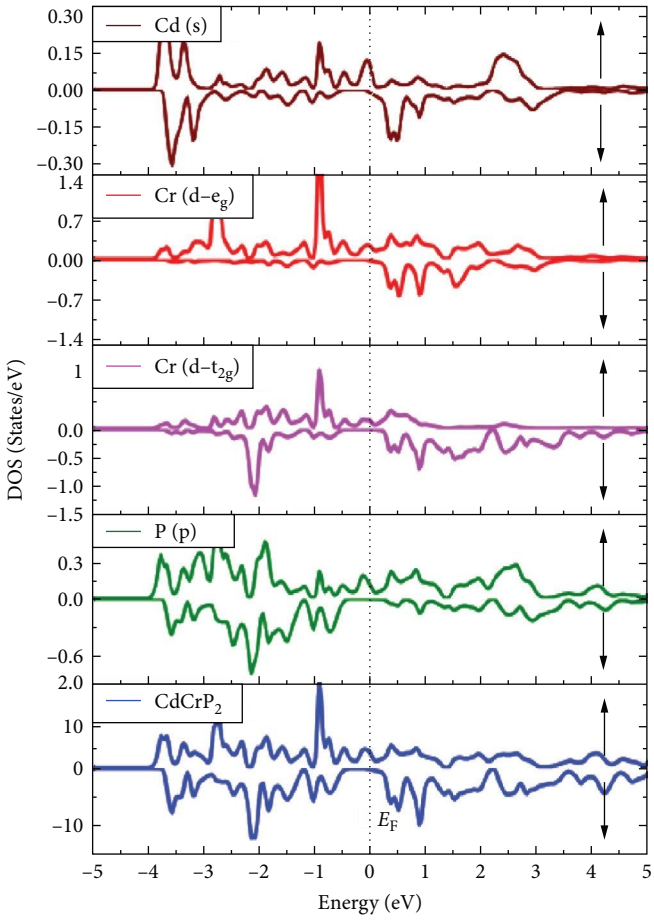

FIGURE 6: Spin-dependent total and partial density of states of $CdCrP_2$ using the generalized gradient approximation (GGA).

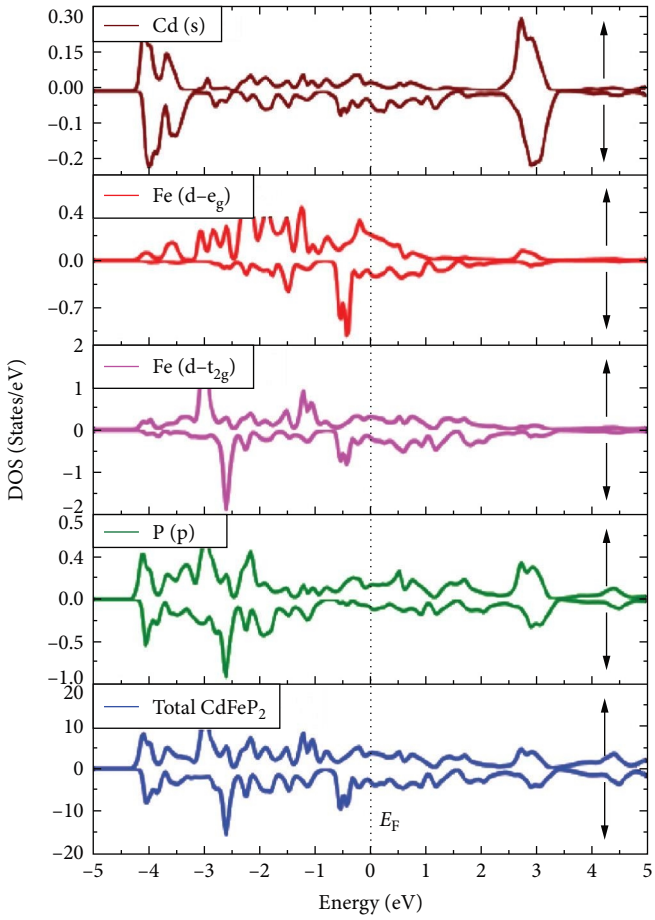

FIGURE 7: Spin-dependent total and partial density of states of $CdFeP_2$ using the generalized gradient approximation (GGA).

Mn, Fe and B = P, As) have been computed within both the LSDA and GGA methods. These results are summarized in Table 5. It is evident from the findings that the primary source of the total magnetic moments stems from the partially filled -3d states of the M atoms. For instance, in $CdCrB_2$, the Cr atom contributes some of its valence electrons to the majority spin band during bond formation, resulting in a total magnetic moment of 2.00 μB/f.u., as shown in Table 5.

Similarly, the Mn atom in $CdMnB_2$ contributes three unpaired d electrons for a total magnetic moment of 3.00 μ_B per formula unit. However, in $CdFeB_2$, the Fe atom's magnetic moment gets reduced due to hybridization and repulsion, resulting in stable ferromagnetism without HMF behavior. The magnetic moments calculated by GGA and LSDA significantly differ, with GGA yielding higher values. Our obtained spin-resolved electronic band structures and charge density analysis provide valuable insights into the electronic and magnetic properties of $CdAB_2$ chalcopyrites, revealing their potential for applications in various fields of materials science.

4. Conclusion

In pursuit of new HMF materials, we conducted comprehensive first-principles calculations on $CdAB_2$ compounds in the chalcopyrite structure within the GGA and LSDA schemes. Ground state properties were evaluated from the energy–volume relation. The $CdAB_2$ compounds were found to be ferromagnetically stable from the total energy calculations. The structural parameters of $CdGeB_2$ host compounds agreed well with existing experimental and theoretical data, no comparative data were available for $CdAB_2$ compounds. The negative formation energies (ΔH) indicated that these compounds are energetically favorable when A occupies the Group IV (Ge) position in $CdGeB_2$.

The spin-polarized calculations unveiled intriguing spin-splitting of energy states near the Fermi level (E_F) upon the substitution of A atoms at the Group IV (Ge) position in $CdGeB_2$. For $CdAB_2$ compounds with A = Cr and Mn, a distinct energy gap was observed around the E_F in the spin-down channel, while the VB crossed the E_F in the spin-up channel, confirming the presence of HMF nature with 100% spin polarization around the E_F. Therefore, the HMF property in $CdAB_2$ (A = Cr, Mn; B = P, As) arose due to the hybridization of A -3d (t_{2g}) and B -3/4p states, with a minor contribution from Cd -s states and their corresponding calculated total magnetic moment were found to be 2.00 μ_B and 3.00 μ_B per formula unit, respectively.

Conversely, in $CdFeB_2$ compounds, the overlapping of wave functions of -3*d* (t_{2g} and e_g) states of Fe and repulsion

with B -*np* states were more pronounced, leading to a reduction in the space charge density of the Fe atom. This effect diminished the possibility of HMF due to the broadening of VBs. The calculated total magnetic moments for $CdFeP_2$ and $CdFeAs_2$ were determined to be 1.83 (1.64 μ_B/f.u.) and 1.94 μ_B/f.u. (1.84 μ_B/f.u.), respectively, under GGA (LSDA) approximations. Consequently, the ground state of $CdFeB_2$ compounds did not exhibit significant HMF characteristics when using LSDA and GGA functionals. However, considerable magnetic properties, such as stable ferromagnetism, were observed in these compounds. In conclusion, our first-principles study sheds light on the potential HMF nature in $CdAB_2$ (A = Cr, Mn; B = P, As) chalcopyrites. These findings hold significance in the ongoing search for novel HMF materials, offering promising avenues for the future spintronics applications.

Data Availability

The data used to support the findings of this study are included within the article.

Conflicts of Interest

The authors declare that they have no conflicts of interest.

References

[1] S. A. Wolf, D. D. Awschalom, R. A. Buhrman et al., "Spintronics: a spin-based electronics vision for the future," *Science*, vol. 294, no. 5546, pp. 1488–1495, 2001.

[2] Y. Chen, W. Mi, J. Yang et al., "Nanostructured electrode materials for advanced sodium-ion batteries," *Solid State Communications*, vol. 12, Article ID 18, 2015.

[3] G. A. Prinz, "Magnetoelectronics," *Science*, vol. 282, no. 5394, pp. 1660–1663, 1998.

[4] B. Doumi, A. Tadjer, F. Dahmane et al., "First-principle investigations of structural, electronic, and half-metallic ferromagnetic properties in $In_{1-B}TM_BP$ (TM = Cr, Mn)," *Journal of Superconductivity and Novel Magnetism*, vol. 27, Article ID 293, 2014.

[5] K. L. Yao, G. Y. Gao, and Z. L. Liu, "Half-metallic ferromagnetism of zinc-blende CrS and CrP: a first-principles pseudopotential study," *Solid State Communications*, vol. 133, no. 5, pp. 301–304, 2005.

[6] J. Yang, F. Xie, Z. Qu, and A. Garfinkel, "Mechanism for spiral wave breakup in excitable and oscillatory media," *Physical Review Letters*, vol. 91, no. 14, Article ID 148302, 2003.

[7] S. Benramache and B. Benhaoua, "Influence of substrate temperature and cobalt concentration on structural and optical properties of ZnO thin films prepared by ultrasonic spray technique," *Superlattices and Microstructures*, vol. 52, no. 4, pp. 807–815, 2012.

[8] N. Azeem, A. Waqas, M. Abdul, and N. Ghulam, "Role and review of educational robotic platforms in preparing engineers for industry," *Journal of Computational Intelligence and Electronic Systems*, vol. 2, no. 1, pp. 1–12, 2014.

[9] M. Hassan, G. Springholz, R. T. Lechner, H. Groiss, R. Kirchschlager, and G. Bauer, "Molecular beam epitaxy of single phase GeMnTe with high ferromagnetic transition temperature," *Journal of Crystal Growth*, vol. 323, no. 1, pp. 363–367, 2011.

[10] S. Cho, S. Choi, G. B. Cha, S. Cheol, and Hong, "Magneto-optic kerr effect and magnetic properties of ferromagnetic semiconducting MnGeAs2 thin films," *Physical Review Letters*, vol. 88, Article ID 257203, 2002.

[11] G. A. Medvedkin, K. Hirose, T. Ishibashi, T. Nishi, V. G. Voevodin, and K. Sato, "MBE growth of MnGeP2 thin films," *Journal of Crystal Growth*, vol. 236, pp. 609–612, 2002.

[12] S. C. Erwin and I. Zutic, "Tailoring ferromagnetic chalcopyrites," *Nature Materials*, vol. 3, pp. 410–414, 2004.

[13] S. Cho, S. Choi, G. B. Cha et al., "Electronic and magnetic properties of MnSnAs2," *Physica Status Solidi (B)*, vol. b241, pp. 1462–1465, 2004.

[14] S. Cho, S. Choi, G. B. Cha et al., "Electronic and magnetic properties of Mn-doped BeSiAs2 and BeGeAs2 compounds," *Solid State Communications*, vol. 129, Article ID 609, 2004.

[15] G. A. Medvedkin, T. Ishibashi, T. Nishi, K. Hayata, Y. Hasegawa, and K. Sato, "Room temperature ferromagnetism in novel diluted magnetic semiconductor Cd1-BMnBGeP2," *Japanese Journal of Applied Physics*, vol. 39, no. 10A, Article ID L949, 2000.

[16] R. Demin, L. Koroleva, S. Marenkin, S. Mikhailov, R. Szymczak, and M. Baran, "Antiferromagnetic–ferromagnetic phase transition in (Zn, Sn, Mn)As_2 epitaBial thin films," *Physica Status Solidi C*, vol. 12, Article ID 3525, 2004.

[17] K. Yoshino, A. Kinoshita, Y. Shirahata, and T. Ikari, "Carrier-induced magnetic anomalies in Mn-doped $AgGaSe_2$ magnetic semiconductor," *Journal of Applied Physics*, vol. 103, no. 7, Article ID 07D103, 2008.

[18] Y. J. Zhao, P. Mahadevan, and A. Zunger, "Comparison of predicted ferromagnetic tendencies of Mn substituting the Ga site in III–V's and in I–III–VI_2, I–III–VI_2 chalcopyrite semiconductors," *Applied Physics Letters*, vol. 84, no. 19, pp. 3753–3755, 2004.

[19] D. Vijayalakshmi and G. Kalpana, "Electronic structure and magnetic properties of chalcopyrite type ZnMB2 (M = Sc, V, Cr, Mn, and Fe; B = P, As) compounds: an ab-initio study," *Physica Status Solidi B*, vol. 253, no. 8, pp. 1576–1584, 2016.

[20] D. Vijayalakshmi and G. Kalpana, "First-principle calculations on structural, electronic, and magnetic properties of CdMAs2 (M = Sc, Ti, V) chalcopyrites," *Canadian Journal of Physics*, vol. 95, no. 11, 2017.

[21] W. Ghazal, S. Mamoun, M. B. Kanoun, S. Goumri-Said, and A. E. Merad, "Electronic, magnetic and optical properties of Cr and Fe doped ZnS and CdS diluted magnetic semiconductors: revised study within TB-mBJ potential," *Optical and Quantum Electronics*, vol. 55, no. 4, Article ID 310, 2023.

[22] Y. J. Zhao, W. T. Geng, K. T. Park, and A. Freeman, "Mn composition dependence of phase stability of $Ga_{1-x}Mn_xAs$ alloys from first principles," *Physical Review B*, vol. 64, Article ID 035207, 2002.

[23] L. A. Siddig, R. H. Alzard, A. S. Abdelhamid et al., "Cobalt hydrogen-bonded organic framework as a visible light-driven photocatalyst for CO_2 cycloaddition reaction," *Inorganic Chemistry*, vol. 62, no. 38, pp. 15550–15564, 2023.

[24] J. P. Perdew and Y. Wang, "Accurate and simple analytic representation of the electron-gas correlation energy," *Physical Review B*, vol. 45, no. 23, Article ID 079904, 1992.

[25] W. Kohn and L. J. Sham, "One-particle properties of an inhomogeneous interacting electron gas," *Physical Review*, vol. 145, no. 2, Article ID 561, 1966.

[26] J. P. Perdew, S. Burke, and M. Ernzerhof, "Generalized gradient approximation made simple," *Physical Review of Letters*, vol. 78, no. 18, Article ID 3865, 1997.

[27] W. Kohn and L. J. Sham, "Self-consistent equations including exchange and correlation effects," *Physical Review*, vol. 140, no. 4A, pp. A1133–A1138, 1965.

[28] J. Rufinus, "Magnetic properties of M-doped (M = Mn, Cr, or V) $ZnSiN_2$," *Journal of Applied Physics*, vol. 105, Article ID 07C509, 2009.

[29] V. M. Novotortsev, A. V. Kochura, and S. F. Marenkin, "New ferromagnetics based on manganese-alloyed chalcopyrites AIIBIVCV2, inorg," *Inorganic Materials*, vol. 46, Article ID 1421, 2010.